J. Phys. B: At. Mol. Opt. Phys. **25** (1992) 4889-4910. Printed in the UK

Differential and integral cross sections for electron impact excitation of the n^3S, n^1S and n^3P ($n = 2, 3$) levels in He

S Trajmar†, D F Register†§, D C Cartwright‡ and G Csanak‡||

† Jet Propulsion Laboratory, California Institute of Technology, Pasadena, CA 91109, USA
‡ Los Alamos National Laboratory, University of California, Los Alamos, NM 87545, USA

Received 2 April 1982, in final form 13 August 1992

Abstract. Differential and integral electron impact excitation cross sections are reported for the n^3S, n^1S and n^3P ($n = 2, 3$) levels in He. Differential cross sections were measured at 30, 50 and 100 eV impact energies in the 10° to 135° angular range, extrapolated to 0 and 180°, and then integrated over all angles to obtain integral cross sections at these three incident electron energies. In addition, differential cross sections were measured for excitation of the n^3S ($n = 2, 3, 4, 5$), n^1S and n^3P ($n = 2, 3, 4$) levels at 60 eV impact energy and 30° scattering angle. Theoretical cross sections based on first-order many-body theory (FOMBT) are also reported for these three final state symmetries for the 30-500 eV impact energy range. These new experimental and theoretical results are compared with other data. In general, good qualitative agreement is found between the experimental and theoretical results but there are quantitative discrepancies in the absolute values obtained by experiment and various theoretical methods at impact energies less than 100 eV.

1. Introduction

Electron collision processes involving He are important in a large variety of systems and environments (various discharge and laser systems, fusion plasmas, planetary and astrophysical environments). From an academic point of view, these collisions represent simple processes that are suitable for theoretical treatment and for developing and refining calculational schemes. A large number of cross section measurements have been reported for He. Available data up to 1978 were surveyed by Bransden and McDowell (1978). Most of these investigations concerned excitations to levels that are optically (dipole) allowed from the ground level. A very recent discussion and updating of these n^1P excitation cross sections and comparison of experimental and theoretical results were given by Cartwright *et al* (1992a).

Cross section data for excitation of optically forbidden transitions are much more limited. Table 1 contains a summary of cross section measurements concerned with excitation of the n^3S, n^1S and n^3P ($n = 2, 3$) levels. Works carried out before 1978 have been in large extent discussed by Bransden and McDowell (1978). A review on cross section data for excitation of the metastable (2^3S, 2^1S) levels at low electron-impact energies was published by Fabrikant *et al* (1988). Only a few new measurements have been reported beyond these two reviews. Sakai *et al* (1989) determined relative (with respect to 2^1P) differential cross sections (DCSs) for excitation of the 2^3S and 2^1S levels

§ Present address: Phillips Petroleum Company, Bartlesville, OK 74003, USA.
|| Present address: Institute of Applied Physics, University of Tsukuba, Tsukuba, Japan.

0953-4075/92/224880+22$07.50

Table 1. Summary of cross section measurements for excitation of the n^3S, n^1S and n^3P ($n = 2, 3$) levels in He.

Reference	Levels	Type	Energy[a] range (eV)	Angular range (deg)
St John *et al* (1964)	3^3S, 3^1S, 3^3P	Q	60, 100, 200	—
Jobe and St John (1967)	2^3P	Q	Tr–450	—
Vriens *et al* (1968)	2^3S, 2^1S	DCS, Q	100–225; 400	5–20
Moussa *et al* (1969)	3^3S, 3^1S, 3^3P	Q	50–6000	—
McConkey and Woosley (1969)	3^3P	Q	24–300	—
van Raan *et al* (1971)	3^3P	Q	20–1500	—
Opal and Beatty (1972)	2^3S, 2^1S, 2^3P	DCS	82, 200	30–150
Rice *et al* (1972)	2^1S	DCS, Q	26.5–81.6	10–80
Brongersma *et al* (1972)	2^3S, 2^1P	Q	19–24	—
Crooks *et al* (1972)	2^3S	DCS	40–70	25–150
Hall *et al* (1973)	2^3S, 2^1S, 2^3P	DCS, Q	29.2, 39.2, 48.2	10–125
Trajmar (1973)	2^3S, 2^1S, 2^3P	DCS, Q	29.6, 40.1	3–138
Suzuki and Takayanagi (1973)	2^3S, 2^1S, 2^3P	DCS	50–500	20–120
Skerbele *et al* (1973)	2^3S, 2^1S	DCS	300–500	0–20
van Raan *et al* (1974)	3^3P	Q	100–1000	—
Chutjian and Srivastava (1975)	2^3P	DCS, Q	60, 80	5–136
Chutjian and Thomas (1975)	3^3S, 3^1S	DCS, Q	29.2, 39.7	5–136
Dillon and Lassettre (1975)	2^1S	DCS	200–700	7.5–35
Dillon (1975)	2^3S	DCS	200–500	7.5–35
Showalter and Kay (1975)	3^3P	Q	60	—
Pichou *et al* (1976)	2^3S, 3^3S	DCS	Tr–23.4	30–120
Yagishita *et al* (1976)	2^3S, 2^3P	DCS	50–500; 200	5–120
Joyez *et al* (1976)	2^3S, 2^1S, 2^3P	DCS	Tr–20.2	6–120
Huetz *et al* (1976)	2^3S	DCS	Tr–23	120
van Zyl *et al* (1980)	3^1S	Q	50–2000	—
Phillips and Wong (1981)	2^3S, 2^1S, 2^3P, 2^1P	DCS	Tr–24	40–90
Johnston and Burrow (1983)	2^3S	Q	20.35	—
Spence *et al* (1983)	2^3S, 2^1S	Q	Tr–23	—
Sakai *et al* (1989)	2^3S, 2^1S	DCS	200–1000	0–16
Brunger *et al* (1990)	2^3S, 2^1S, 2^3P	DCS	29.6, 40.1	2–90
Sakai *et al* (1991)	2^3S	DCS	200, 500; 200–800	0–12; 0

[a] Tr stands for threshold.

at small scattering angles (θ) in the 200–1000 eV impact energy (E) range. They found that these cross sections increase as the scattering angle decreases to 0°, especially in the case of the 2^3S excitation. In a more recent study (Sakai *et al* 1991) they applied high angular resolution and studied the 2^3S DCS behaviour in the 0°–12° angular range at impact energies of 200 and 500 eV and at 0° at impact energies ranging from 200–800 eV. This study confirmed the sharp rise of the DCS near 0° and yielded normalized DCS values. Brunger *et al* (1990) measured relative (to 2^1P) differential scattering intensities for the 2^3S, 2^1S and 2^3P excitations at 29.6 and 40.1 eV impact energies in the 2°–90° angular range (and determined absolute DCS values for the 2^1P excitation at 29.6 eV at scattering angles ranging from 5°–100°). Integral cross sections (ICS) for excitation of the 2^3S level were determined in the threshold to 19.8 eV impact energy range by Johnston and Burrow (1983), and for excitation of the 2^3S and 2^1S levels, from threshold to 3 eV above threshold, by Spence *et al* 1983). van Zyl *et al* (1980) deduced integral electron-impact excitation cross sections for the n^1S ($n = 3$–6)

levels from benchmark optical emission measurements in the 50–2000 eV impact energy range. They exercised great care to minimize experimental errors and estimated the uncertainty to be a few per cent (3.5% at 500 eV) in their results. Although the list in table 1 looks extensive, it has to be emphasized that there are large gaps in DCS data in the energy and angular ranges for the 3^3S and 3^1S excitations and no measurements have been reported for excitation of the 3^3P level.

The theoretical methods used for the excitation of the 2^3S, 2^1S and 2^3P levels of helium and the comparison of the results with experimental data have been discussed by Bransden and McDowell (1977, 1978) and by Fabrikant *et al* (1988). The implementation of various perturbative methods has been discussed by Walters (1984) and distorted wave approximation results have been reviewed by Itikawa (1986). Results from calculations using 10-state coupled-channels-optical (Brunger *et al* 1990), close-coupling (Bhadra *et al* 1979), *R*-matrix (Fon *et al* 1979, 1988, 1991, Nakazaki *et al* 1991), distorted-wave optical potentials (Baluja and McDowell 1979) and eikonal theory (Mansky and Flannery 1990) are available.

We report here experimentally derived differential and integral electron-impact cross sections for excitation of the n^3S, n^1S and n^3P ($n = 2, 3$) levels measured at 30, 50 and 100 eV impact energies and corresponding theoretical results obtained using first-order many-body theory (FOMBT) in the 30–500 eV impact energy range. The present experimental and theoretical results are compared with each other and with other available results to assess the applicability of the FOMBT for these excitation processes. This work is a continuation of our previous efforts to determine the excitation cross sections of He and quantitatively evaluate the applicability of FOMBT.

We also determined differential cross sections at 60 eV impact energy and 30° scattering angle from a high-resolution energy-loss spectrum for excitation of the m^3S, n^1S, n^3P ($m = 2, 3, 4$ and 5; $n = 2$, 3 and 4) levels for the purpose of comparison with theoretical calculations.

Excitation of the 3^1D and 3^3D levels cannot be resolved from excitation of the 3^1P level in conventional energy-loss spectra with presently available energy resolution but only by the application of electron–photon coincidence techniques. We have not included in table 1 measurements concerning these excitation processes and excitations to $n > 3$ levels for which only some integral cross sections (from optical measurements) are available. Estimation of the cross sections for excitation of the 3^1D levels will be reported by Cartwright *et al* (1992b).

2. Experimental methods

The differential cross sections were determined from conventional electron-impact, energy-loss spectra obtained in beam–beam scattering experiments at 30, 50, 60 and 100 eV impact energies and scattering angles ranging from 10° to 135°. Typical energy-loss spectra demonstrating the drastic variation of relative excitation probabilities with scattering angle are shown in figure 1. The electron-impact spectrometer and experimental procedures utilized in the present measurements have been described earlier (Trajmar and Register 1984, Cartwright *et al* 1977); therefore, only a brief summary is given here. Electrons were extracted from a hot tungsten filament. A nearly monoenergetic electron beam was formed using a double-hemispherical energy selector and cylindrical electrostatic lens systems. This electron beam crossed at right angles by an He beam effusing from a capillary array. The aspect ratio (length to diameter) for

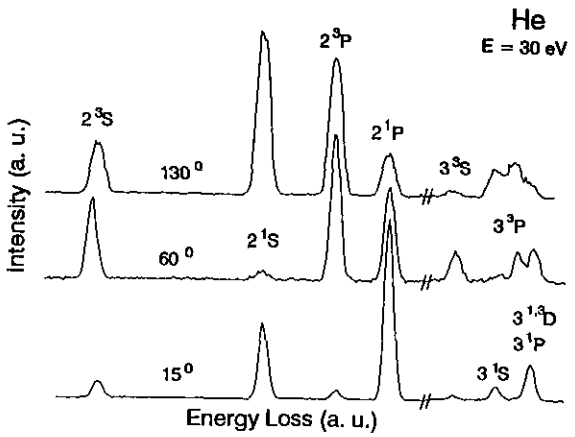

Figure 1. Energy-loss spectra at $E = 30$ eV, $\theta = 15$, 60 and 130°.

individual capillaries was 100 and the diameter of the array containing about 100 individual capillaries was 0.75 mm. Detailed descriptions of this capillary array and characteristics of the beam formed by them have been given by Brinkmann and Trajmar (1981). The He gas pressure behind the capillary array was typically 5 Torr as measured by a calibrated capacitance manometer. The background pressure in the vacuum chamber was about 10^{-6} Torr. Electrons scattered by nominal angle θ into a solid angle ($\Delta\Omega$) of about 10^{-3} sr were detected as a function of energy loss. The detector consisted of a double-hemispherical energy analyser and cylindrical lens system, similar to those in the electron gun. The overall resolution of the apparatus was set to about 50 meV (FWHM) to obtain a good compromise between resolution and signal levels. Energy-loss spectra covering the $n = 2$ and 3 manifold excitations were obtained at fixed E and θ values by pulse-counting, multichannel-scaling techniques. The impact-energy scale was calibrated on the 19.37 eV resonance in the elastic scattering channel at 90° scattering angle, and the true scattering angle was determined from the symmetry of the scattering signal for the 2^1P excitation around 0°. Special care was exercised to avoid dependence of electron detection sensitivity on residual energy of the scattered electrons. This was achieved by sweeping the voltages on two elements of the detector lens system simultaneously with the energy-loss sweep. The nature of these voltage sweeps was determined by optimizing the response function of the detector both for the minimum and the maximum values of electron residual energies appearing in the spectrum. Details of the lens system and operation have been given by Chutjian (1974) and Trajmar and Register (1984).

The small background contribution was subtracted from the energy-loss spectra based on scattering detected between the energy-loss features. From the energy-loss spectra (after background correction) the relative scattering intensities of individual inelastic features with respect to that of the 2^1P feature were determined by computer fitting and integrating the scattering signal under individual features. The inputs to the least-squares fitting procedure were the energy-loss values corresponding to various excitations and the lineshape function (which was taken to be the same as for the 2^1P excitation feature). Utilizing these relative intensities and the DCSs for the 2^1P level excitation, as given by Cartwright *et al* (1992a), we obtained absolute DCSs for the n^3S, n^1S and n^3P ($n = 2$ and 3) excitations.

One energy-loss spectrum was also taken at $E = 60$ eV, $\theta = 30°$ with an overall energy resolution of about 18 meV (FWHM) to resolve some of the $n = 4$ and 5 energy-loss features and to obtain some information for comparison with theoretical results (see figure 2).

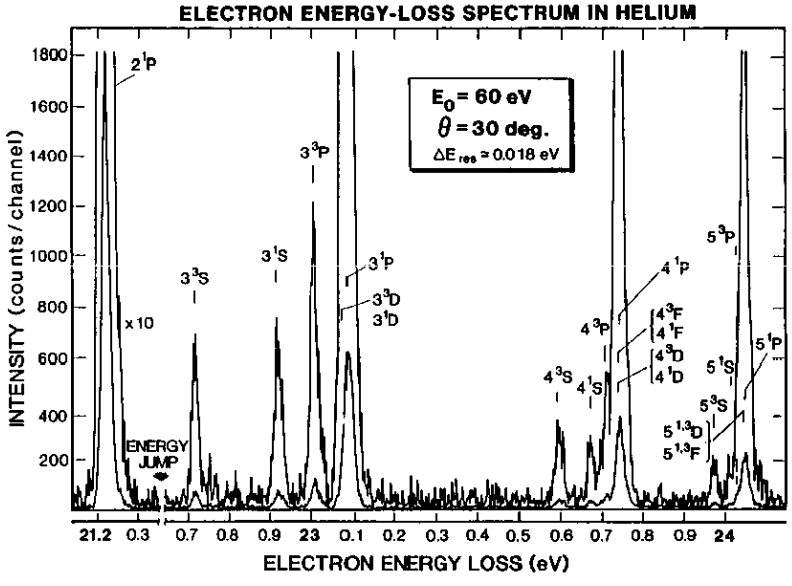

Figure 2. High-resolution energy-loss spectrum at $E = 60$ eV, $\theta = 30°$.

3. Theoretical foundations

First-order many-body theory (FOMBT) applied to the description of electron-atom inelastic scattering was first introduced by Csanak *et al* (1971). Many-body theory in this lowest-order form can be considered to be one of many possible forms of the distorted wave approximation (DWA). It is important to emphasize that while there are many different ways to introduce a distortion potential in the DWA, there is only a *single* FOMBT that is consistent with the foundations of many-body theory. This FOMBT incorporates static and exchange distortion effects on the free-electron wavefunctions in a well-prescribed fashion, and the inelastic scattering T-matrix consists of direct and exchange scattering amplitudes. The fundamental formulae of FOMBT and their application in describing excitation of the atomic states of He have been reported earlier (Thomas *et al* 1973, 1974, Meneses and Csanak 1987), and only a brief summary will be given here.

The inelastic scattering T-matrix for excitation of He in FOMBT is given by the formula

$$T^{\mathrm{FOMBT}}_{\tilde{0}\tilde{p},\tilde{n}\tilde{q}} = \int \mathrm{d}x_1\, \mathrm{d}x_2\, f^{(-)\mathrm{HF}*}_{\tilde{q}}(x_1) f^{(+)\mathrm{HF}}_{\tilde{p}}(x_2)\, V_{\tilde{0}\tilde{n}}(x_1 x_2) \tag{1}$$

where $\tilde{p} \equiv (\boldsymbol{p}, m_s)$ and $\tilde{q} \equiv (\boldsymbol{q}, m'_s)$ refer to the linear momentum $(\boldsymbol{p}, \boldsymbol{q})$ and spin coordinates (m_s, m'_s) of the incident and scattered electrons; $f^{(+)\mathrm{HF}}_{\tilde{p}}(x)$ and $f^{(-)\mathrm{HF}}_{\tilde{q}}(x)$ are the

continuum Hartree-Fock (HF) (i.e. static-exchange) orbitals for an electron with momentum $\tilde{p}$ in the field of the He atom, with outgoing and incoming wave boundary conditions (respectively); $\bar{0}$ and $\bar{n}$ refer to the collection of quantum numbers of the initial (ground) and final (excited) He states, respectively; and the symbols x_1, x_2 refer to the combined spatial (r_1, r_2) and spin (σ_1, σ_2) coordinates of the electrons.

The quantity $V_{\bar{0}\bar{n}}(x_1, x_2)$ is defined by the formula (using Hartree atomic units)

$$V_{\bar{0}\bar{n}}(x_1, x_2) = \delta(x_1 - x_2) \int \frac{\mathrm{d}r'}{|r_1 - r'|} X^{\mathrm{RPA}}_{\bar{n}}(x', x') - \frac{1}{|r_1 - r_2|} X^{\mathrm{RPA}}_{\bar{n}}(x_1, x_2) \tag{2}$$

where $X^{\mathrm{RPA}}_{\bar{n}}(x_1, x_2)$ is the random phase approximation (RPA) for the transition density matrix between states $\bar{n}$ and $\bar{0}$, $\delta(x_1 - x_2) = \delta(r_1 - r_2)\delta_{\sigma_1\sigma_2}$ where $\delta(r_1 - r_2)$ is the Dirac delta function, and $\delta_{\sigma_1\sigma_2}$ is the Kronecker delta. The transition density matrix $X_{\bar{n}}(x, x')$ between states $\bar{n}$ and $\bar{0}$ using wavefunction terminology, is defined by the formula

$$X_{\bar{n}}(x, x') = N \int \Psi^*_{\bar{n}}(x, x_2, \ldots, x_N)\Psi_{\bar{0}}(x', x_2, \ldots, x_N)\,\mathrm{d}x_2, \ldots, \mathrm{d}x_N \tag{3}$$

where $\Psi_{\bar{0}}(x_1, x_2, \ldots, x_N)$ and $\Psi_{\bar{n}}(x_1, x_2, \ldots, x_N)$ refer to the ground ($\bar{0}$) and excited ($\bar{n}$) state wavefunctions of the atomic system, respectively.

It has also been shown that for the $n^1\mathrm{P}$ ($n = 2, 3$) excited levels of He, the RPA transition density is well approximated by taking $\Psi_{\bar{0}}$ in the HF approximation, and $\Psi_{\bar{n}}$ in the fixed-core HF (FCHF) approximation. This calculational scheme was adopted here in the case of the excitation of $n^3\mathrm{S}$ and $n^3\mathrm{P}$ ($n = 2, 3, \ldots, 6$) levels of He as well, but a somewhat different approach was used for the $n^1\mathrm{S}$ ($n = 2, 3, \ldots$) excitation calculations.

Thus, in the case of $n^3\mathrm{S}$ and $n^3\mathrm{P}$ ($n = 2, 3, \ldots$) levels we obtain for the transition density matrix the form

$$X_{n^3L_{M_L M_S}}(x, x') = \tfrac{1}{2}\phi^*_{n_L M_L}(r)\phi_{1s}(r')\zeta^*_{1M_S}(\sigma, \sigma') \tag{4}$$

where $\phi_{n_L M_L}(r)$ is the one-electron FCHF orbital and the $\zeta_{S,M_S}(\sigma, \sigma')$ spin function is defined by the formula

$$\zeta_{S,M_S}(\sigma, \sigma') = \sum_{m_1 m_2} (-1)^{\frac{1}{2}+m_1} C^{\frac{1}{2}\frac{1}{2}S}_{-m_1 m_2 M_S} \eta_{m_1}(\sigma)\eta^*_{m_2}(\sigma') \tag{5}$$

where $\eta_m(\sigma)$ is the Pauli spin function. In obtaining (4) we assumed that the $\phi_{n_L M_L}(r)$ orbital is orthogonal to the $\phi_{1s}(r)$ orbital, which is obvious for the $L = 1$ case, and can be chosen that way for the $L = 0$ case. Using (4) in (2) we obtain for $n^3L_{M_L M_S}$ excitation

$$V_{\bar{0},n^3L_{M_L M_S}}(x_1, x_2) = -\frac{1}{|r_1 - r_2|} \tfrac{1}{2}\phi^*_{n_L M_L}(r)\phi_{1s}(r_1)\zeta^*_{1M_S}(\sigma_1, \sigma_2) \tag{6}$$

which in turn gives for the T-matrix

$$\begin{aligned} T^{\mathrm{FOMBT}}_{\bar{0}\tilde{p},n^3L_{M_L M_S}\tilde{q}} &= \frac{(-1)^{\frac{1}{2}+m'_s}}{2\sqrt{2}} \int \mathrm{d}r_1 \int \mathrm{d}r_2 f^{(-)\mathrm{HF}*}_q(r_1) f^{(+)\mathrm{HF}}_p(r_2) \frac{1}{|r_1 - r_2|} \\ &\quad \times \phi^*_{nLM_L}(r_2)\phi_{1s}(r_1) C^{\frac{1}{2}\frac{1}{2}S}_{-m'_s m_s M_S} \\ &\equiv -\frac{1}{2\sqrt{2}} T^{\mathrm{E}}_{M_L}(-1)^{m_s - \frac{1}{2}} C^{\frac{1}{2}\frac{1}{2}S}_{-m'_s m_s M_S} \end{aligned} \tag{7}$$

where we introduced $T^{\mathrm{E}}_{M_L}$ by the definition

$$T^{\mathrm{E}}_{M_L} = \int \mathrm{d}r_1 \int \mathrm{d}r_2 f^{(-)\mathrm{HF}*}_q(r_1) f^{(+)\mathrm{HF}}_p(r_2) \frac{1}{|r_1 - r_2|} \phi^*_{n_L M_L}(r_2)\phi_{1s}(r_1). \tag{8}$$

As we can see immediately from (7), the excitation of a ^3S or ^3P level can occur only through exchange.

In the case of n^1S ($n=2, 3, \ldots$) excitation, the usual fixed-core HF approximation does not give a good result and the simplest and most accurate method is to follow a representation introduced by Cohen and McEachran (Cohen and McEachran 1967, McEachran and Cohen 1969, Crothers and McEachran 1970). In this representation the $S=0$ states of helium are described by the following wavefunctions:

$$\Psi_{n^1L_{M_L}}(x_1, x_2) = N_{nL}[\phi_0(r_1)\phi_{n_LM_L}(r_2)+\phi_0(r_2)\phi_{n_LM_L}(r_1)] \times\frac{1}{\sqrt{2}}[\alpha(\sigma_1)\beta(\sigma_2)-\beta(\sigma_1)\alpha(\sigma_2)] \tag{9}$$

where N_{nL} is a normalization constant and $\phi_0(r)$ is the normalized 1s orbital of He^+ and can be given as (using Hartree atomic units)

$$\phi_0(r)=2^{5/2}\,e^{-2r}Y_{00}(r). \tag{10}$$

The $\phi_{nLM_L}(r)$ orbitals were obtained by Cohen and McEachran (1967) by solving the fixed core HF equations with $\phi_0(r)$ being *fixed* as given by (10). Cohen and McEachran (1967) have fitted numerically the $\phi_{nLM_L}(r)$ orbitals in the following form:

$$\phi_{nLM_L}(r)=\sum_{n=L+1}^{J-L} B_N^{nL}\,e^{-\beta r}r^{N-1}Y_{LM_L}(\hat{r}) \tag{11}$$

and they have tabulated the B_N^{nL} coefficients for $n=1$, 2 and 3. We note here that in the Cohen-McEachran (1967) scheme the 1^1S ground state is also represented in the form given by (9) (with $n=1$, $L=M_L=0$). From (9) we obtain for the normalization constant

$$N_{nL}=[2(1+|S_{nL,0}|^2)]^{-1/2} \tag{12}$$

where

$$S_{nL,0}=\int d\boldsymbol{r}\,\phi^*_{nLM_L}(\boldsymbol{r})\phi_0(\boldsymbol{r}) \tag{13}$$

is an overlap integral.

If we use the wavefunctions given by equations (9) and (10) in (3) for $\bar{n}=n^1S$, $\bar{0}=1^1S$, we obtain

$$X_{n^1S}(r\sigma, r'\sigma') = N_{1S}N_{nS}\{\phi_0(r)\phi^*_{ns}(r')S_{0,1s}+\phi_{1s}(r)\phi^*_0(r')S_{0,ns}+\phi_{1s}(r)\phi^*_{ns}(r')\} \times[\alpha^*(\sigma')\alpha(\sigma)+\beta^*(\sigma')\beta(\sigma)] \tag{14}$$

where we introduced the notation

$$S_{0,ns}=\int \phi^*_0(r_2)\phi_{ns}(r_2)\,dr_2 \tag{15}$$

for the overlap integral. If we assume on the right-hand side of (14) that

$$S_{0,ns}\approx 0 \qquad \text{for } n>1 \tag{16}$$

then we obtain

$$X_{n^1S}(\boldsymbol{r},\sigma,\boldsymbol{r}'\sigma')$$

$$\approx N_{1S}N_{nS}\{\phi_{1s}(\boldsymbol{r})\phi^*_{ns}(\boldsymbol{r}')S^2_{0,1s}+\phi_{1s}(\boldsymbol{r})\phi^*_{ns}(\boldsymbol{r}')\}[\alpha^*(\sigma')\alpha(\sigma)+\beta^*(\sigma')\beta(\sigma)]$$

$$= N_{1S}N_{nS}(1+S^2_{0,1s})\phi_{1s}(\boldsymbol{r})\phi^*_{ns}(\boldsymbol{r}')[\alpha^*(\sigma')\alpha(\sigma)+\beta^*(\sigma')\beta(\sigma)]$$

$$\approx \tfrac{1}{2}(1+S^2_{0,1s})^{1/2}\phi_{1s}(\boldsymbol{r})\phi^*_{ns}(\boldsymbol{r}')[\alpha^*(\sigma')\alpha(\sigma)+\beta^*(\sigma')\beta(\sigma)]$$

$$\equiv \frac{1}{\sqrt{2}}C_{1s}\phi_{1s}(\boldsymbol{r})\phi^*_{ns}(\boldsymbol{r}')[\alpha^*(\sigma')\alpha(\sigma)+\beta^*(\sigma')\beta(\sigma)]. \tag{17}$$

The nice feature of the approximation given by (17) is that the orthogonality of the 1^1S and n^1S states, expressed by the identity

$$\int X_n(\boldsymbol{r}\sigma,\boldsymbol{r}\sigma)\,\mathrm{d}\boldsymbol{r}\,\mathrm{d}\sigma = 0 \tag{18}$$

is *preserved*, since both the ϕ_{1s} and ϕ_{ns} orbitals are obtained from the same eigenvalue equation with differing eigenvalues and are, therefore, orthogonal. Equation (17) shows that even for n^1S excitation a single-term, factorized representation of $X_{\bar{n}}(\boldsymbol{r},\boldsymbol{r}')$ can be maintained if the factor functions are properly defined. In the calculations reported here we used the form given by (17), in which the $\phi_{1s}(\boldsymbol{r})$ and $\phi_{ns}(\boldsymbol{r})$ orbitals were obtained from the fixed-core HF program of Bates (1974) keeping the $\phi_0(\boldsymbol{r})$ orbital fixed.

Inserting (16) into (2), we obtain

$$V_{\bar{0},n^1S}(x_1x_2) = \delta(x_1-x_2)C_{1s}\sqrt{2}\int\frac{\phi^*_{ns}(\boldsymbol{r}')\phi_{1s}(\boldsymbol{r}')\,\mathrm{d}\boldsymbol{r}'}{|\boldsymbol{r}_1-\boldsymbol{r}'|}-\frac{1}{|\boldsymbol{r}_1-\boldsymbol{r}_2|}\frac{1}{\sqrt{2}}C_{1s}\phi^*_{ns}(\boldsymbol{r}_2)\phi_{1s}(\boldsymbol{r}_1)$$

$$\times\{\alpha^*(\sigma_1)\alpha(\sigma_2)+\beta^*(\sigma_1)\beta(\sigma_2)\} \tag{19}$$

which in turn gives for the T-matrix (via equation (1))

$$T^{\mathrm{FOMBT}}_{\bar{0}\bar{p},n^1S\bar{q}} = C_{1s}\sqrt{2}\int\mathrm{d}\boldsymbol{r}_1\int\mathrm{d}\boldsymbol{r}_2\,f^{(-)\mathrm{HF}*}_q(\boldsymbol{r}_1)f^{(+)\mathrm{HF}}_p(\boldsymbol{r}_1)\frac{\phi_{ns}(\boldsymbol{r}_2)\phi_{1s}(\boldsymbol{r}_2)}{|\boldsymbol{r}_1-\boldsymbol{r}_2|}$$

$$-\frac{C_{1s}}{\sqrt{2}}\int\mathrm{d}\boldsymbol{r}_1\int\mathrm{d}\boldsymbol{r}_2\,f^{(-)\mathrm{HF}*}_q(\boldsymbol{r}_1)f^{(+)\mathrm{HF}}_p(\boldsymbol{r}_2)\frac{1}{|\boldsymbol{r}_1-\boldsymbol{r}_2|}\phi^*_{ns}(\boldsymbol{r}_2)\phi_{1s}(\boldsymbol{r}_1) \tag{20}$$

and where we have assumed the spin factorization

$$f^{(+)\mathrm{HF}}_p(x) = f^{(+)\mathrm{HF}}_p(\boldsymbol{r})\eta_{m_s}(\sigma) \tag{21a}$$

$$f^{(-)\mathrm{HF}}_q(x) = f^{(-)\mathrm{HF}}_q(\boldsymbol{r})\eta_{m_s}(\sigma) \tag{21b}$$

for the continuum HF orbitals, with $\eta_{m_s}(\sigma)$ denoting the Pauli spin functions. The first term on the right-hand side of (20) describes the 'direct' electron excitation process; the second term is associated with the 'exchange' electron excitation process.

If we define T^{D} (the 'direct' excitation T-matrix) and T^{E} (the 'exchange' excitation T-matrix) by the equations

$$T^{\mathrm{D}} = C_{1s}\int\mathrm{d}\boldsymbol{r}_1\int\mathrm{d}\boldsymbol{r}_2 f^{(-)\mathrm{HF}*}_q(\boldsymbol{r}_1)f^{(+)\mathrm{HF}}_p(\boldsymbol{r}_1)\frac{1}{|\boldsymbol{r}_1-\boldsymbol{r}_2|}\phi^*_{ns}(\boldsymbol{r}_2)\phi_{1s}(\boldsymbol{r}_2) \tag{22a}$$

$$T^{\mathrm{E}} = C_{1s}\int\mathrm{d}\boldsymbol{r}_1\int\mathrm{d}\boldsymbol{r}_2 f^{(-)\mathrm{HF}*}_q(\boldsymbol{r}_1)f^{(+)\mathrm{HF}}_p(\boldsymbol{r}_2)\frac{1}{|\boldsymbol{r}_1-\boldsymbol{r}_2|}\phi_{ns}(\boldsymbol{r}_1)\phi_{1s}(\boldsymbol{r}_2) \tag{22b}$$

then (19) can be rewritten as

$$T_{\hat{0}\hat{p},n^1\mathrm{S}\hat{q}} = \sqrt{2}(T^{\mathrm{D}} - \tfrac{1}{2}T^{\mathrm{E}})\delta_{m_s m_s'}. \tag{23}$$

In calculating T^{D} and T^{E} it is convenient to expand both $f_p^{(+)\mathrm{HF}}(\boldsymbol{r})$ and $f_q^{(-)\mathrm{HF}}(\boldsymbol{r})$ in terms of incident electronic partial waves according to

$$f_p^{(+)\mathrm{HF}}(\boldsymbol{r}) = \sum_{l_p=0}^{\infty} \mathrm{i}^{l_p} \cos\delta_{l_p}^{\mathrm{HF}}(p)\, \mathrm{e}^{\mathrm{i}\delta_{l_p}^{\mathrm{HF}}(p)} P_{p,l_p}(r) P_{l_p}(\cos\theta) \tag{24a}$$

and

$$f_q^{(-)\mathrm{HF}}(\boldsymbol{r}) = \frac{4\pi}{qr} \sum_{l_q=0}^{\infty} \sum_{m_q=-l_q}^{l_q} \mathrm{i}^{l_q} \cos\delta_{l_q}^{\mathrm{HF}}(q)\, \mathrm{e}^{\mathrm{i}\delta_{l_q}^{\mathrm{HF}}(q)} P_{q,l_q}(r)\, Y_{l_q m_q}^*(\hat{q})\, Y_{l_q m_q}(\hat{r}). \tag{24b}$$

We have chosen the incident electron direction as the positive z-axis; θ is the polar angle of $\boldsymbol{r}$, and $\hat{r}$ and $\hat{q}$ refer to the angular coordinates of $\boldsymbol{r}$ and $\boldsymbol{q}$, respectively. Without loss of generality, the scattered electron can be assumed to propagate in the (x, z) plane so that the azimuthal angle of the scattered electron. (This coordinate system is frequently referred to as the 'collision frame.') The functions $P_{p,l_p}(r)$ and $P_{q,l_q}(r)$ are the appropriate radial continuum HF orbitals with associated phaseshifts $\delta_{l_p}^{\mathrm{HF}}(p)$ and $\delta_{l_q}^{\mathrm{HF}}(q)$, respectively; $P_l(z)$ refers to the usual Legendre polynomial; and $Y_{lm}(\hat{r})$ is the customary spherical harmonic.

Inserting (10*a*, *b*) into (8*a*, *b*) and writing the target orbitals in the form

$$\phi_{1\mathrm{s}}(\boldsymbol{r}) = \frac{P_{1\mathrm{s}}(r)}{r} Y_{00}(\hat{r}) \tag{25a}$$

and

$$\phi_{n\mathrm{s}}(\boldsymbol{r}) = \frac{P_{n\mathrm{p}}(r)}{r} Y_{00}(\hat{r}) \tag{25b}$$

we obtain

$$T^{\mathrm{D}} = -\frac{4\pi}{pq}\mathrm{i} \sum_{l_p l_q} (-1)^{\frac{1}{2}(l_p - l_q)}\, \mathrm{e}^{\mathrm{i}\Delta(p,l_p;q,l_q)} \frac{2l_q+1}{\sqrt{3}} C_{000}^{l_q\,0\,l_p} C_{000}^{l_q\,0\,l_p} T^{\mathrm{D}}_{p,l_p,q,l_q} P_{l_q}(\cos\theta_q) \tag{26}$$

and

$$T^{\mathrm{E}} = -\frac{4\pi}{pq}\mathrm{i} \sum_{l_p l_q} (-1)^{\frac{1}{2}(l_p - l_q)}\, \mathrm{e}^{\mathrm{i}\Delta(p,l_p;q,l_q)} \sqrt{3}\, C_{000}^{l_q\,0\,l_p} C_{000}^{l_q\,0\,l_p} T^{\mathrm{E}}_{p,l_p,q,l_q} P_{l_q}(\cos\theta_q) \tag{27}$$

where

$$\Delta(p, l_p, q, l_q) \equiv \delta_{l_p}(p) + \delta_{l_q}(q).$$

We have also introduced the following definitions for the 'direct' and 'exchange' radial integrals:

$$T^{\mathrm{D}}_{p,l_p,q,l_q} = \int_0^\infty \int_0^\infty P_{p,l_p}(r_1) P_{q,l_q}(r_1) v_0(r_1, r_2) P_{1\mathrm{s}}(r_2) P_n(r_2)\, \mathrm{d}r_1\, \mathrm{d}r_2 \tag{28}$$

$$T^{\mathrm{E}}_{p,l_p,q,l_q} = \int_0^\infty \int_0^\infty P_{p,l_p}(r_1) P_n(r_1) v_{l_q}(r_1, r_2) P_{1\mathrm{s}}(r_2) P_{q,l_q}(r_2)\, \mathrm{d}r_1\, \mathrm{d}r_2 \tag{29}$$

where $v_\lambda(r_1, r_2)$ is the λth term in the multipole expansion of the $(1/|\boldsymbol{r}_1 - \boldsymbol{r}_2|)$ Coulomb interaction potential.

The evaluation of T^D and T^E, using partial-wave expansions, are described in more detail in Cartwright *et al* (1992a). It turns out that T^E can be evaluated accurately and relatively quickly using spline-integration techniques but T^D (needed for n^1S excitation) requires substantially more numerical effort to obtain accurate results. This is because the 'transition potential' is much longer range than the exchange equivalent (Cartwright *et al* 1992a). Specifically, the inner and outer integrals were calculated using spline-fitting and spline-integration methods. In the calculation of the exchange integrals, one of the functions is always of a bound-state type and therefore only limited integration-range needed to be considered for both the r_1 and r_2 integrals. Availability of Cray YMP computers allowed the utilization of a very fine integration grid guaranteeing high numerical accuracy.

The magnetic sublevel ($M = 0, \pm 1$) differential cross sections are identified here as

$$\left(\frac{d\sigma}{d\Omega}\right)_{M_L} = \frac{q}{4\pi^2 p}\,\tfrac{1}{2}|2T^D_{M_L} - T^E_{M_L}|^2 \tag{30}$$

where for n^1S excitation $T^D_0 \equiv T^D$ and $T^E_0 \equiv T^E$ and the total (summed over magnetic sublevels) level differential cross section is obtained from

$$\left(\frac{d\sigma}{d\Omega}\right) = \sum_{M_L}^{L}\left(\frac{d\sigma}{d\Omega}\right)_{M_L} = \left(\frac{d\sigma}{d\Omega}\right)_{M_L=0} + 2\left(\frac{d\sigma}{d\Omega}\right)_{M_L=1}. \tag{31}$$

The numerical accuracy of the computer codes used to obtain the theoretical results reported in this research was verified by comparing the corresponding differential and integral cross sections with the earlier FOMBT results of Thomas *et al* (1974). The agreement is generally excellent, and any small differences from the earlier FOMBT results can be attributed to small differences in the helium bound-state orbitals.

4. Results and discussion

The experimental DCSs obtained in the present work at 30, 50 and 100 eV impact energies are summarized in tables 2, 3 and 4, respectively. The average error associated with the DCS and ICS is given at the bottom of each DCS column. In the estimation of error limits, we considered statistical errors associated with the individual features and the errors specified for the 2^1P DCS by Cartwright *et al* (1992a). The total error was obtained as the square root of the sum of the squares of the contributing errors. Integral cross sections obtained by extrapolation and integration of the DCSs from 0° to 180° are also given in the tables. The extrapolation was aided by theory and this procedure may introduce an additional error of about 5%. When combined with the DCS errors, this results in an increase of the total error by about 1%.

In table 5 we compare DCSs obtained from the 60 eV, 30° high-resolution, energy-loss spectrum with the results from FOMBT.

In figures 3–9 the present experimental and FOMBT DCS results are shown and compared with other experimental and theoretical results. Similar comparisons are made for the integral cross sections in figures 10–14.

The quantity that is measured most reliably in the present experiments is the ratio of the scattering intensity associated with a given inelastic process to that of the 2^1P excitation. These ratios are nearly identical to the corresponding DCS ratios. The instrument response function for the various $n = 2, 3$ excitations can be taken to be the same at these impact energies and the different angular behaviours have only minor

Table 2. Experimental cross sections at $E = 30$ eV. DCS (10^{-16} cm^2 sr^{-1}).

θ (deg)	2^3S	2^1S	2^3P	3^3S	3^1S	3^3P
10	3.68^{-3}	2.45^{-2}	1.87^{-3}	1.09^{-3}	3.68^{-3}	5.70^{-4}
15	3.47^{-3}	1.59^{-2}	1.83^{-3}	8.98^{-4}	2.54^{-3}	6.16^{-4}
20	3.12^{-3}	9.7^{-3}	1.80^{-3}	8.49^{-4}	1.66^{-3}	5.59^{-4}
30	2.0^{-3}	2.49^{-3}	1.97^{-3}	5.99^{-4}	4.30^{-4}	4.46^{-4}
40	1.10^{-3}	2.80^{-4}	2.0^{-3}	3.79^{-4}	8.79^{-5}	3.23^{-4}
50	1.23^{-3}	3.36^{-5}	2.22^{-3}	3.60^{-4}	6.96^{-5}	3.25^{-4}
60	1.23^{-3}	1.18^{-4}	2.39^{-3}	4.06^{-4}	8.58^{-5}	4.06^{-4}
70	1.52^{-3}	2.65^{-4}	2.35^{-3}	5.86^{-4}	9.57^{-5}	3.79^{-4}
80	1.84^{-3}	4.52^{-4}	2.34^{-3}	6.67^{-4}	1.01^{-4}	4.22^{-4}
90	1.70^{-3}	6.83^{-4}	2.39^{-3}	5.91^{-4}	6.0^{-5}	4.22^{-4}
100	1.37^{-3}	1.12^{-3}	2.55^{-3}	4.27^{-4}	1.21^{-4}	5.13^{-4}
110	8.49^{-4}	1.57^{-3}	2.51^{-3}	2.46^{-4}	2.07^{-4}	4.76^{-4}
120	7.69^{-4}	2.20^{-3}	2.63^{-3}	1.21^{-4}	3.25^{-4}	5.75^{-4}
130	1.30^{-3}	3.87^{-3}	2.94^{-3}	1.25^{-4}	5.73^{-4}	7.5^{-4}
140	3.17^{-3}	6.96^{-3}	3.25^{-3}	4.03^{-4}	1.23^{-3}	9.46^{-4}
DCS errors	21%	20%	19%	22%	29%	23%
			Q (10^{-16} cm^2)			
	2.44^{-2}	3.92^{-2}	3.20^{-2}	5.80^{-3}	6.70^{-3}	7.20^{-3}

Table 3. Experimental cross sections at $E = 50$ eV. DCS (10^{-16} cm^2 sr^{-1}).

θ (deg)	2^3S	2^1S	2^3P	3^3S	3^1S	3^3P
5	4.36^{-3}	4.91^{-2}	—	—	9.68^{-3}	—
10	3.55^{-3}	2.56^{-2}	1.05^{-3}	6.65^{-4}	4.73^{-3}	3.48^{-4}
15	3.10^{-3}	1.33^{-2}	1.32^{-3}	6.10^{-4}	2.16^{-3}	4.17^{-4}
20	2.71^{-3}	6.52^{-3}	1.87^{-3}	6.03^{-4}	1.01^{-3}	5.46^{-4}
30	1.65^{-3}	1.73^{-3}	2.9^{-3}	4.58^{-4}	1.97^{-4}	6.63^{-4}
40	6.38^{-4}	5.0^{-4}	3.83^{-3}	2.17^{-4}	1.48^{-4}	8.03^{-4}
50	1.81^{-4}	1.71^{-4}	3.01^{-3}	9.01^{-5}	3.8^{-5}	7.69^{-4}
60	4.5^{-5}	3.77^{-4}	2.42^{-3}	5.2^{-5}	2.7^{-5}	6.61^{-4}
70	1.4^{-5}	7.28^{-4}	1.77^{-3}	3.1^{-5}	7.7^{-5}	4.89^{-4}
80	9.1^{-6}	1.11^{-3}	1.35^{-3}	1.70^{-5}	1.74^{-4}	4.28^{-4}
90	5.3^{-6}	1.32^{-3}	1.10^{-3}	7.7^{-6}	2.32^{-4}	3.48^{-4}
100	7.4^{-5}	1.53^{-3}	9.5^{-4}	8.3^{-6}	3.07^{-4}	3.16^{-4}
110	2.74^{-4}	1.59^{-3}	7.58^{-4}	4.00^{-5}	3.60^{-4}	2.50^{-4}
120	6.04^{-4}	1.79^{-3}	6.77^{-4}	1.3^{-4}	3.96^{-4}	2.23^{-4}
130	1.10^{-3}	2.09^{-3}	5.66^{-4}	2.45^{-4}	4.87^{-4}	2.22^{-4}
140	1.33^{-3}	1.80^{-3}	3.11^{-4}	3.15^{-4}	4.19^{-4}	9.71^{-5}
DCS errors	22%	15%	16%	18%	18%	16%
			Q (10^{-16} cm^2)			
	8.65^{-3}	2.31^{-2}	1.75^{-2}	2.15^{-3}	4.40^{-3}	4.84^{-3}

Table 4. Experimental cross sections at $E = 100$ eV. DCS (10^{-16} cm^2 sr^{-1}).

θ (deg)	2^3S	2^1S	2^3P	3^3S	3^1S	3^3P
5	1.52^{-3}	4.97^{-2}	—	—	8.86^{-3}	—
10	1.07^{-3}	2.12^{-2}	5.66^{-4}	2.03^{-4}	3.64^{-3}	—
15	7.85^{-4}	1.18^{-2}	8.39^{-4}	1.81^{-4}	2.07^{-3}	1.44^{-4}
20	3.78^{-4}	6.25^{-3}	8.76^{-4}	9.8^{-5}	1.27^{-3}	1.70^{-4}
30	9.59^{-5}	1.56^{-3}	7.05^{-4}	1.8^{-5}	3.66^{-4}	2.07^{-4}
40	5.12^{-5}	6.19^{-4}	5.07^{-4}	4.73^{-6}	1.44^{-4}	1.71^{-4}
50	6.81^{-5}	4.4^{-4}	2.83^{-4}	1.08^{-5}	8.8^{-5}	8.56^{-5}
60	7.7^{-5}	5.0^{-4}	1.69^{-4}	1.60^{-5}	1.05^{-4}	5.02^{-5}
70	6.64^{-5}	4.61^{-4}	1.033^{-4}	1.42^{-5}	9.87^{-5}	3.47^{-5}
80	5.74^{-5}	4.16^{-4}	6.28^{-5}	9.0^{-6}	8.95^{-5}	2.18^{-5}
90	4.15^{-5}	2.66^{-4}	3.49^{-5}	9.3^{-6}	6.54^{-5}	5.6^{-6}
100	5.53^{-5}	2.97^{-4}	2.69^{-5}	1.27^{-5}	7.01^{-5}	4.9^{-6}
110	6.19^{-5}	2.62^{-4}	2.33^{-5}	1.38^{-5}	5.74^{-5}	6.6^{-6}
120	7.94^{-5}	2.23^{-4}	1.55^{-5}	1.76^{-5}	5.98^{-5}	3.1^{-6}
130	8.17^{-5}	1.90^{-4}	1.11^{-5}	2.01^{-5}	4.43^{-5}	4.4^{-6}
140	9.54^{-5}	1.82^{-4}	9.34^{-6}	1.93^{-5}	4.77^{-5}	—
DCS errors	14%	10%	15%	24%	12%	50%
			Q (10^{-16} cm^2)			
	1.26^{-3}	1.24^{-2}	1.89^{-3}	2.50^{-4}	2.51^{-3}	5.80^{-4}

Table 5. DCS obtained from 60 eV, 30° energy-loss spectrum shown in figure 1 and FOMBT.

	DCS (10^{-20} cm^2 sr^{-1})	
Level	Expt	FOMBT
3^3S	4.2	0.665
3^1S	4.0	14.4
3^3P	7.8	15.5
4^3S	2.0	0.273
4^1S	1.5	5.72
4^3P	2.5	6.49
5^3S	1.2	0.136

influence on the corresponding effective scattering volumes (see Brinkmann and Trajmar 1981). For the $n = 2$ manifold these ratios have been measured recently at 29.6 eV impact energy by Brunger *et al* (1990) and their results are compared with the present ones at 30 eV in figure 3(a). The agreement is generally excellent between the two sets of experimental data except for a small angular range near 60°. The corresponding results predicted by FOMBT are also shown in figure 3(a), and generally the theory overestimates these ratios. For the $n = 3$ manifold DCS ratios, we compare the present 30 eV values with those of Chutjian and Thomas (1975) measured at 29.2 eV impact energy. The agreement between the two ratios is generally good although there are substantial disagreements at a few angles especially near the deep minimum for the

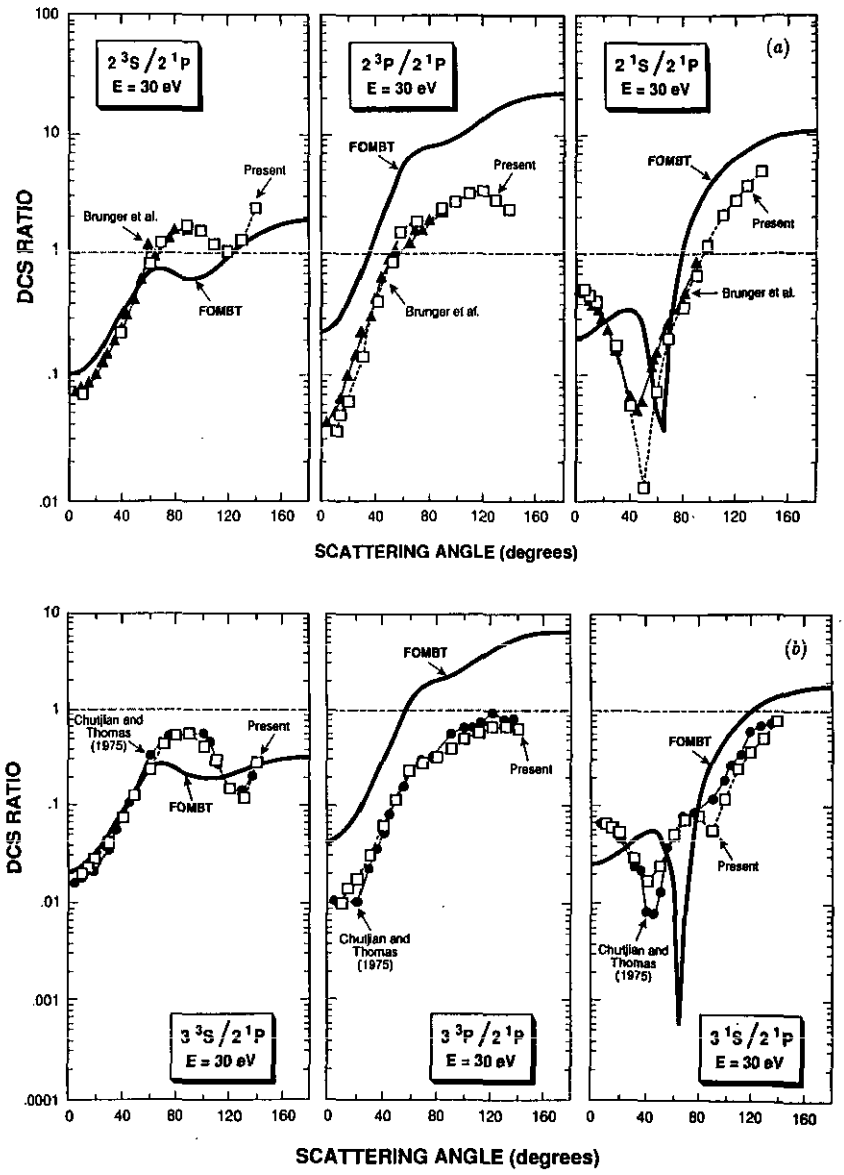

Figure 3. (*a*) Comparison of $n = 2$ manifold DCS ratios. Experimental data: ▲, Brunger *et al* (1990) at 29.6 eV; □, present. FOMBT calculations: full curves. (*b*) Same as (*a*) except for the $n = 3$ levels, and the experimental results (●) are from Chutjian and Thomas (1975).

3^1S excitation cross section. Ratios predicted by the FOMBT calculations are in reasonable agreement except for the $3^3P/2^1P$ ratio which is about a factor of two larger than experiment. Chutjian and Thomas (1975) also reported these ratios at 39.7 eV impact energy. Comparisons with those data will be made in a subsequent publication (Cartwright *et al* 1992b).

Differential excitation cross sections for the 2^3S level are shown in figure 4. At impact energies for which experimental data are available from more than one laboratory, the agreement is in general good although in some regions disagreements greater

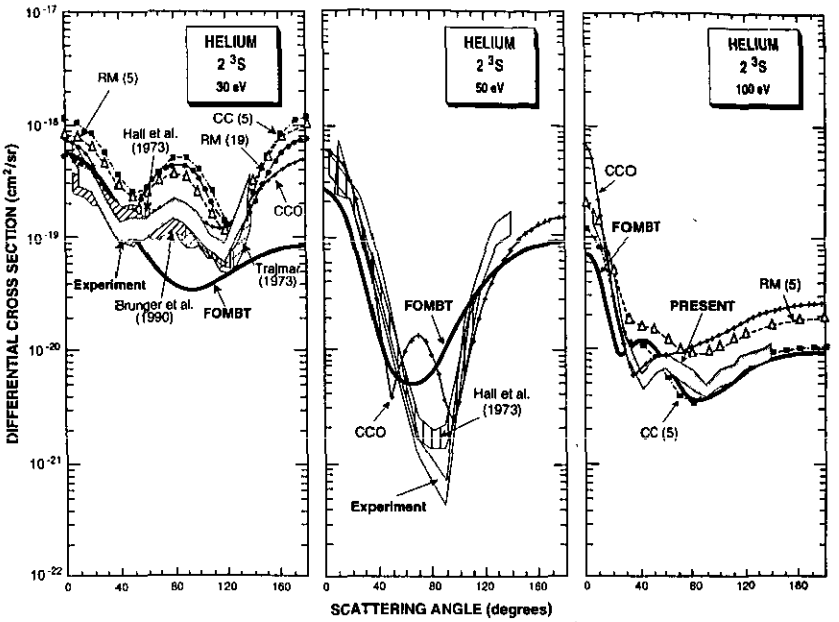

Figure 4. Comparison of present experimental and FOMBT results with selected other theoretical and experimental results for the electron impact excitation DCS of the 2^3S level of helium with $E = 30$ eV (left panel), $E = 50$ eV (middle panel) and $E = 100$ eV, right panel) incident energy electrons. Other experimental results shown are: Hall *et al* (1973), Trajmar (1973) and Brunger *et al* (1990) all at 29.6 eV. (Shaded regions represent the error limits.) Other theoretical results shown are: 5-state *R*-matrix theory (RM (5)) results of Fon *et al* (1979), 19-state *R*-matrix theory (RM (19)) results of Fon *et al* (1988), the 10-state coupled-channels-optical calculation (CCO) results of Brunger *et al* (1990), and the 5-state close coupling calculation (CC (5)) results of Bhadra *et al* (1979).

than the combined error limits exist. The same remarks can be made for the 2^1S and 2^3P experimental DCSs shown in figures 5 and 6, respectively.

As can be seen from figure 4 for the $1^1S \rightarrow 2^3S$ excitation, none of the current theoretical methods, including the most elaborate ones, predict both the magnitude and the shape of the measured DCSs at 30, 50 and 100 eV impact energies. The quality of the FOMBT results improves as the incident electron energy increases. At 30 eV incident electron energy the 5-state close-coupling results, the 5-state *R*-matrix results, and the 19-state *R*-matrix results all agree with respect to shape with the experimental results but are too large by about a factor of 2. At 30 eV the CCO results are very close to experiment, both in shape and magnitude but the deep minima in the DCS indicated by the CCO calculations at 40 and 81.6 eV impact energies (not shown here) are not supported by the experimental data. As shown in figure 4, even the most elaborate calculations cannot yet reproduce the experimental results for this transition. There are no results shown from eikonal type theories (e.g. Mansky and Flannery 1990). These theories do not treat exchange correctly and, therefore, cannot be used for pure exchange excitation processes.

Figure 5 shows DCS results for the electron impact induced $1^1S \rightarrow 2^1S$ transition and, in this case, the FOMBT results agree qualitatively with the experimental data at all energies. For this transition there is a good agreement for the CCO results with experiment at 50 eV incident electron energy. The very deep minimum in the 2^1S DCS

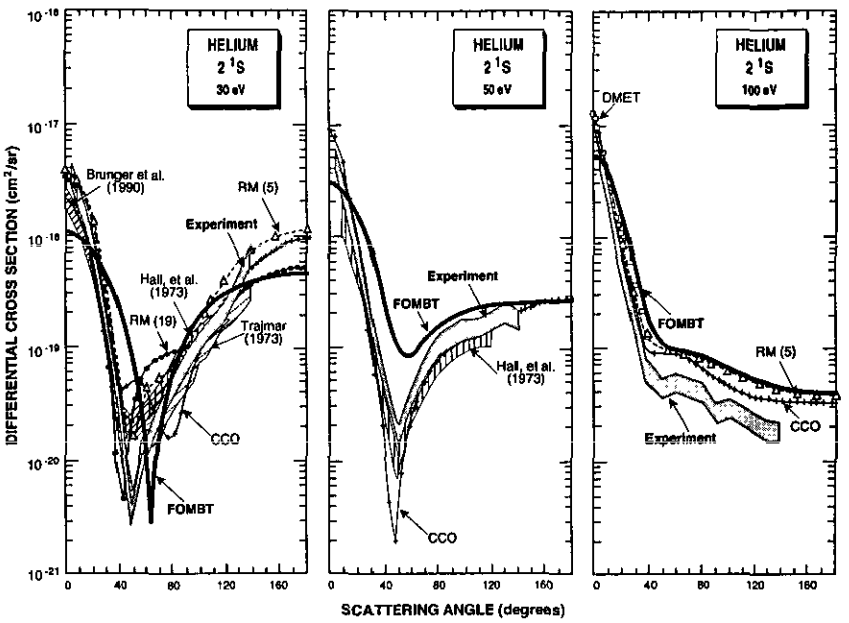

Figure 5. DCSs for excitation for the 2^1S level at impact energies of *30* (left panel), *50* (middle panel) and 100 eV (right panel). The notation is the same as in figure 4. The RM (5) results shown here are from Fon *et al* (1979). The designation DMET refers to the recent 10-channel eikonal theory results of Mansky and Flannery (1990).

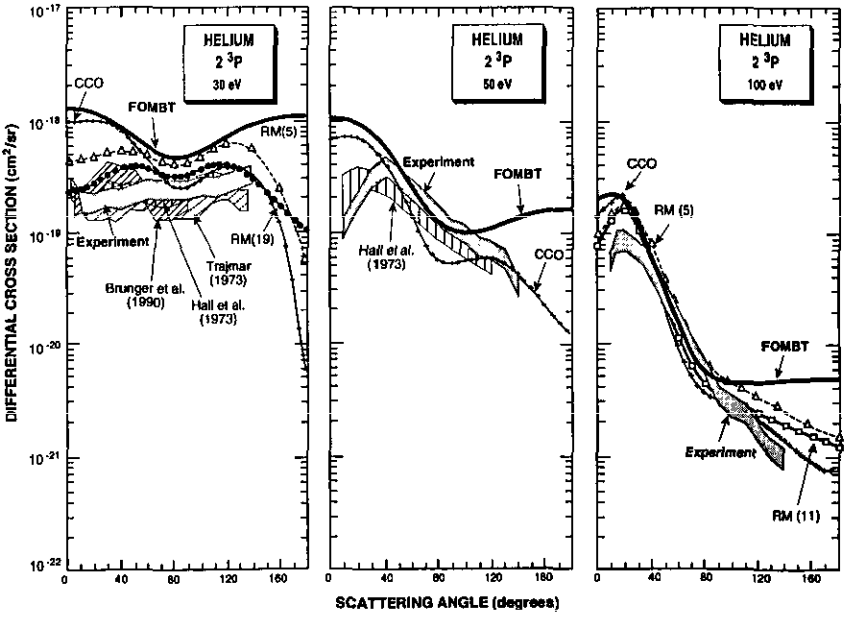

Figure 6. DCSs for excitation of the 2^3P level at *30* (left panel), *50* (middle panel) and 100 eV (right panel) impact energies. The notation is the same as in figure 4 except the RM (19) results are from Fon *et al* (1991). The theoretical results of Nakazaki *et al* (1991) RM (11), are also shown.

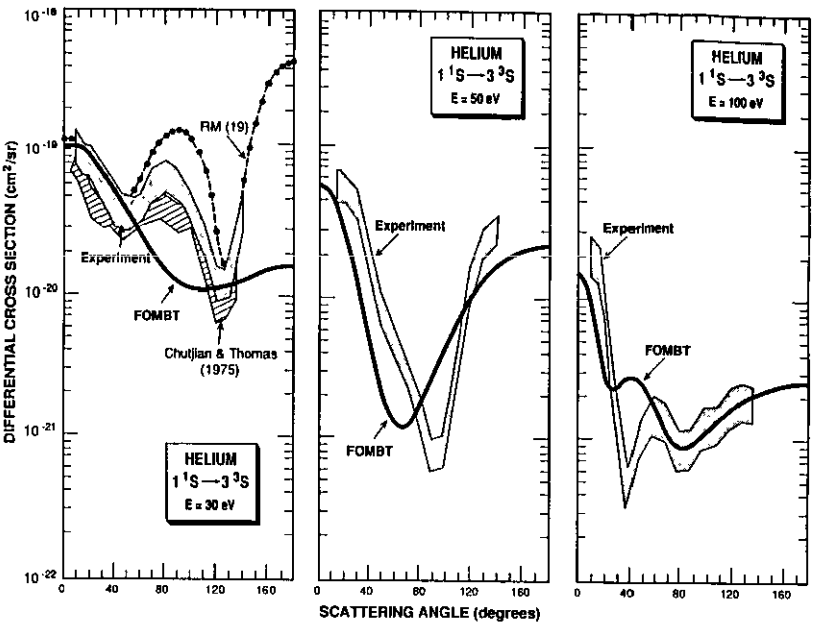

Figure 7. DCSs for excitation of the 3^3S level at 30, (left panel) 50, (middle panel) and 100 eV (right panel) impact energies. The present experimental results and those of Chutjian and Thomas (1975) are shown by the shaded areas representing the error limits. The full curves are the results of the FOMBT calculations. RM (19) refers to the 19 state R-matrix theory results of Fon *et al* (1988).

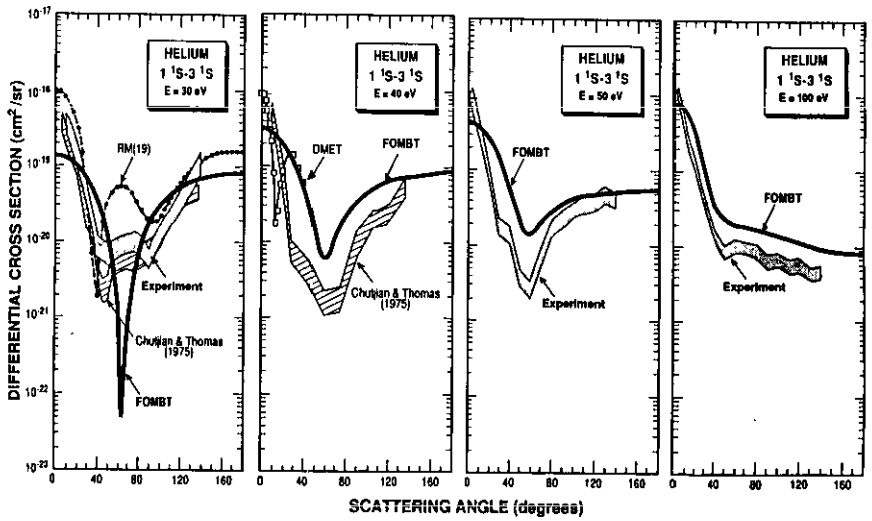

Figure 8. DCSs for excitation of the 3^1S level at 30, 40, 50 and 100 eV impact energies. Notation is the same as for figure 7. In addition the DMET results of Mansky and Flannery (1990) are also shown at 40 eV.

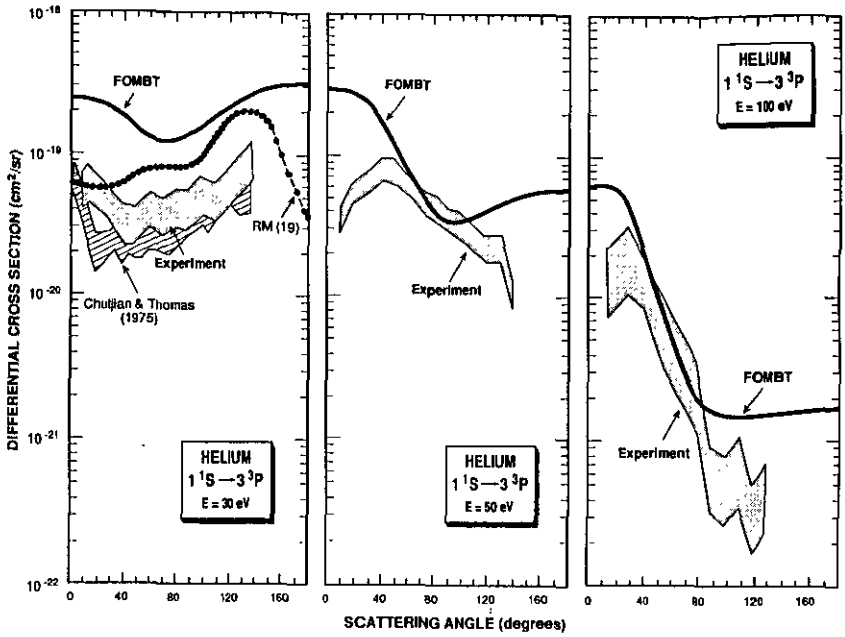

Figure 9. DCS for excitation of the 3^3P level at 30, 50 and 100 eV impact energies. Notation is the same as for figure 7 except the RM (19) results are from Fon *et al* (1991).

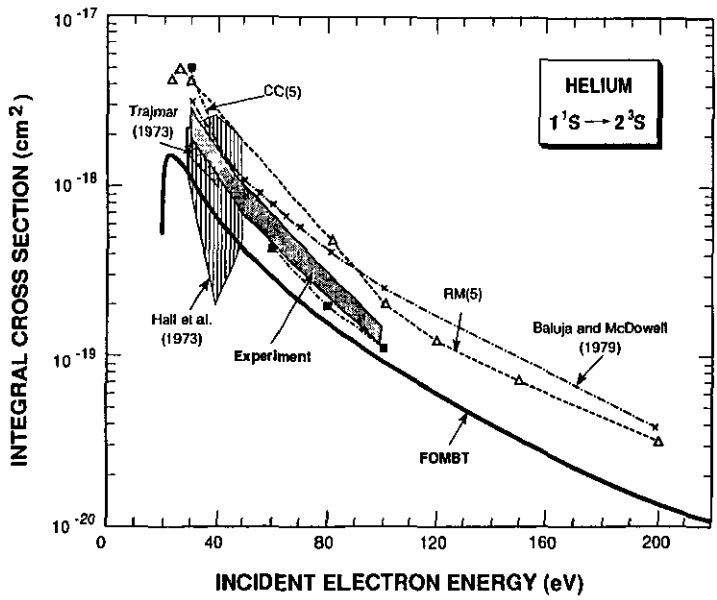

Figure 10. Integral cross sections for excitation of the 2^3S level. Experimental results with error limits are shown from Hall *et al* (1973), Trajmar (1973) and from the present measurements. Theoretical results are: from Baluja and McDowell (1979), and from Fon *et al* (1979) indicated as RM (5). The results indicated by CC (5) refer to the 5-state close coupling calculation results of Bhadra *et al* (1979).

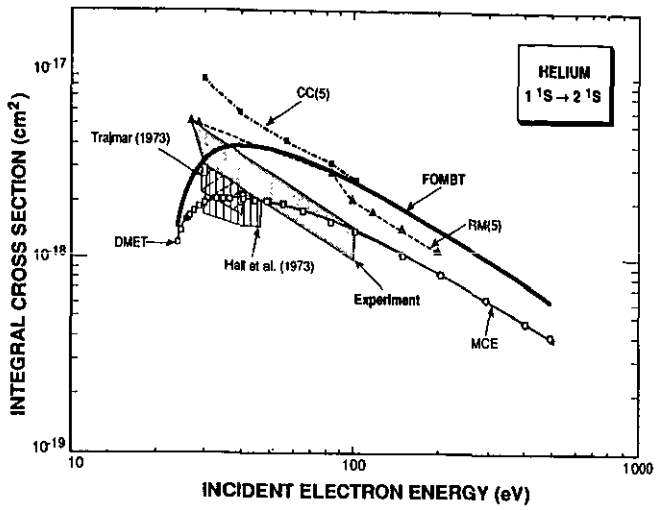

Figure 11. *Same as figure 10 except for the* 2^1S *level. The designations* DMET (rectangles) and MEC (diamonds) refer to the 10-channel eikonal theory results of Mansky and Flannery (1990) and Flannery and McCann (1975), respectively.

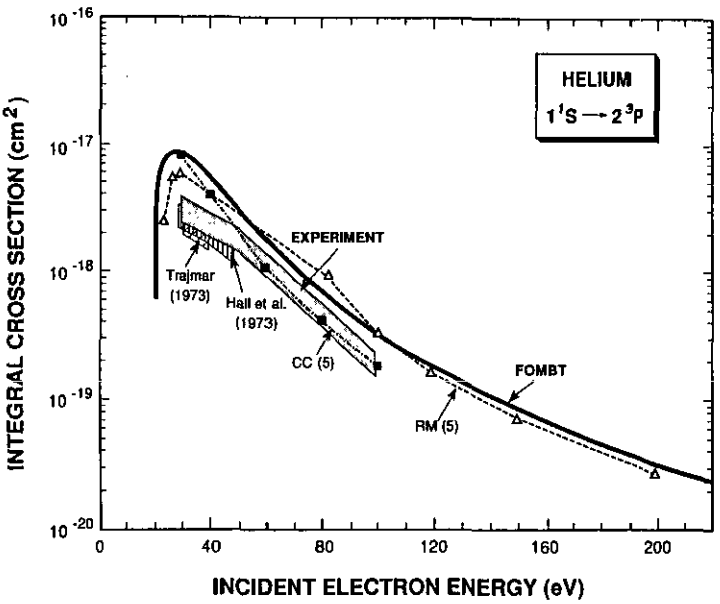

Figure 12. Same as figure 10 except for the 2^3P level.

indicated by the experimental data at 30 eV impact energy is also indicated by the FOMBT, RM (19) and RM (5) theories but the agreement between theory and experiment is not quantitative. It is interesting to note that our FOMBT results agree extremely well with the 5-state R-matrix calculation results and with the eikonal (DMET) results at $E = 100$ eV incident electron energy except for $\theta \leqslant 10°$ scattering angles. This suggests that channel coupling is important at this energy for only $\theta \leqslant 10°$ scattering angles.

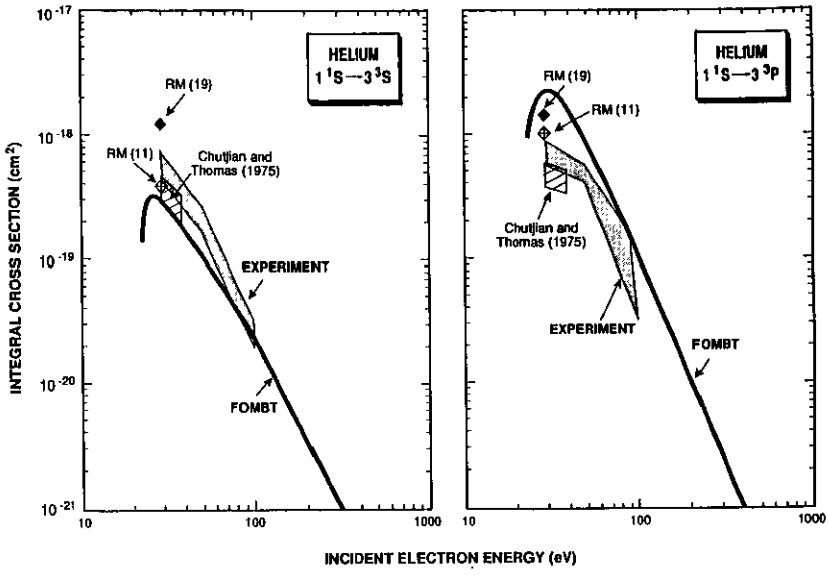

Figure 13. Same as figure 10 except for the 3^3S and 3^3P levels. The experimental results of Chutjian and Thomas (1975) and the theoretical results RM (11) of Nakazaki *et al* (1991) and RM (19) of Fon *et al* (1991) are also shown.

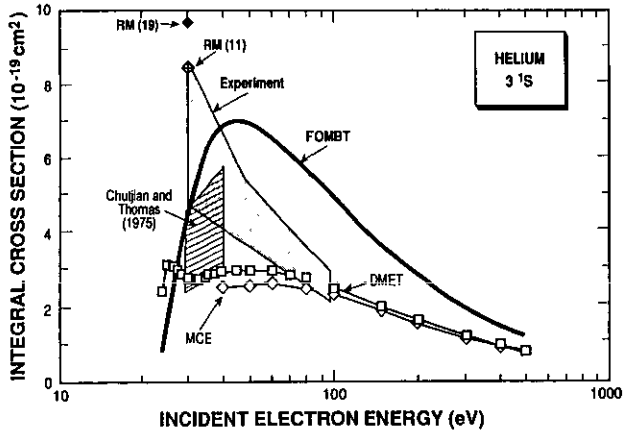

Figure 14. Same as figure 13 except for the 3^1S level.

DMET results are not reported for scattering angles greater than about 40° because exchange contribution may be important at higher angles and it is not properly treated by this theory.

The $1^1S \rightarrow 2^3P$ results are shown in figure 6. At low impact energies the 19-state R-matrix calculations are in the closest agreement with experimental data but too large by about a factor of two. The R-matrix methods predict the proper angular distribution at 100 eV but the DCS values are higher than those obtained by experiment at low and high scattering angles. Again results from eikonal theory are omitted because of the

problems of treating exchange. The CCO results are consistent with experiment at 50 eV, except for low ($\theta \leq 40°$) angles but are surprisingly different from the experimental data at 30 eV both in shape and magnitude. The observed decrease in the DCS at large scattering angles is predicted qualitatively correctly by the CCO and RM theories, but not by FOMBT, and this suggests that channel coupling may be important for this excitation process in this angular region. The FOMBT results for this excitation are too large at the lower impact energies but at 100 eV, in the 40–90° angular range, agreement with experiment is very good. Below and above this angular range the FOMBT results are too high even at this energy.

For the $n = 3$ manifold DCS (figures 7–9) the only other experimental data with which the present results can be compared are those of Chutjian and Thomas (1975), at 29.2 and 39.7 eV impact energies. At low impact energies the 19-state R-matrix results are in the best qualitative agreement with experiments but the predicted DCS are, generally, too large but not quite so much as with FOMBT. At the higher energies the FOMBT results show good qualitative, and even quantitative, agreement with experimental data. Eikonal theory DCS for the 3^1S excitation are reported only at small scattering angles ($\theta \leq 40°$) at 40 eV (figure 8). It predicts a deep minimum at $\theta \approx 10°$ which is not observed experimentally.

Integral cross sections for the $n = 2$ and 3 levels are summarized and compared in figures 10–14. The experimental results overlap within their respective error limits but the energy ranges covered are rather limited. No *general* conclusion appears obvious concerning the reliability of the various theoretical approaches for all transitions, except to note that predictions from the eikonal type theories (DMET and MCE) are generally smaller than both experiment and results from other theories. The 5-channel close coupling theory gives the best agreement with experiments for the 2^3S and 2^3P excitations but predicts too large cross sections for the 2^1S excitations. The FOMBT results are too small for the n^3S, about right for the n^3P and too large for the n^1S excitation when compared to experiment.

5. Conclusions

Differential and integral electron-impact excitation cross sections, derived from experimental data, are reported for the n^3S, n^1S and n^3P ($n = 2, 3$) levels in helium, at 30, 50 and 100 eV impact energies. Theoretical cross sections based on FOMBT are compared with these experimental results and other theoretical results. None of the theoretical results predict both the magnitude and the shapes of the DCSs for the $n = 2$ levels at 30, 50 and 100 eV, although some models agree better with experiment than others at certain energies. The results from many-body theory agree with experiment about as well as the results obtained by solving the close-coupling equations except at 30 eV. Eikonal-type theories, which do not currently include electron exchange (and therefore cannot treat excitation to n^3S, n^3P, n^3D) do not predict reliable DCSs for n^1S except for both high electron energy (200 eV) and scattering angles less than 40°. The 5-channel close-coupling integral results agree best with experiment for 2^3S and 2^3P but substantially over-estimate the 2^1S cross section. These new experimental data will hopefully serve to motivate continual theoretical work to try and develop a better understanding as to what are the dominant physical processes in inelastic electron scattering at low and intermediate energies.

Acknowledgments

David C Cartwright and George Csanak gratefully acknowledge the financial support of the US DOE, the NSF (OIP) and the University of California (Riverside)-Los Alamos National Laboratory Collaborative Research Program (CALCOR) for this study. Partial support for Sandor Trajmar, JPL, Caltech by NASA is acknowledged. Special thanks go to Bernadette Fernandez and Dorothy Hatch for their excellent assistance in preparing the text and figures and editing this paper.

References

Baluja K L and McDowell M R C 1979 *J. Phys. B: At. Mol. Phys.* **12** 835
Bates G N 1974 *Comput. Phys. Commun.* **8** 220
Bhadra K, Callaway J and Henry R J W 1979 *Phys. Rev.* A **19** 1841
Bransden B H and McDowell M R C 1977 *Phys. Rep.* **30C** 207
—— 1978 *Phys. Rep.* **46** 249
Brinkmann R T and Trajmar S 1981 *J. Phys. E: Sci. Instrum.* **19** 245
Brongersma H H, Knoop F W E and Backx C 1972 *Chem. Phys. Lett.* **13** 16
Brunger M J, McCarthy I E, Ratnavelu K, Teubner P J O, Weigold A M, Zhou Y and Allen L J 1990 *J. Phys. B: At. Mol. Opt. Phys.* **23** 1325
Cartwright D C, Chutjian A, Trajmar S and Williams W 1977 *Phys. Rev.* A **16** 1013
Cartwright D C, Csanak G, Trajmar S and Register D F 1992a *Phys. Rev.* A **45** 1602
Cartwright D C, Csanak G and Trajmar S 1992b *Phys. Rep.* in preparation
Chutjian A 1974 *J. Chem. Phys.* **61** 4279
Chutjian A and Srivastava S K 1975 *J. Phys. B: At. Mol. Phys.* **8** 2360
Chutjian A and Thomas L D 1975 *Phys. Rev.* A **11** 1583
Cohen M and McEachran R P 1967 *Proc. Phys. Soc.* **92** 37
Crooks G B, Dubois R D, Golden D E and Rudd M E 1972 *Phys. Rev. Lett.* **29** 327
Crothers D S F and McEachran R P 1970 *J. Phys. B: At. Mol. Phys.* **3** 976
Csanak G, Taylor H S and Yaris R 1971 *Phys. Rev.* A **3** 1322
Dillon M A 1975 *J. Chem. Phys.* **63** 2035
Dillon M A and Lassettre E N 1975 *J. Chem. Phys.* **62** 2373
Fabrikant I I, Shpenik O B, Snegursky A V and Zavilopulo A N 1988 *Phys. Rep.* **159** 1
Flannery M R and McCann K J 1975 *J. Phys. B: At. Mol. Phys.* **8** 1716
Fon W C, Berrington K A, Burke P G and Kingston A E 1979 *J. Phys. B: At. Mol. Phys.* **12** 1861
Fon W C, Berrington K A and Kingston A E 1988 *J. Phys. B: At. Mol. Opt. Phys.* **21** 2961
—— 1991 *J. Phys. B: At. Mol. Opt. Phys.* **24** 2161
Hall R I, Joyez G, Mazeau J, Reinhardt J and Schermann C 1973 *J. Physique* **34** 827
Huetz A, Cresteau F, Joyez G, Mazeau J and Pichou F 1976 *J. Phys. B: At. Mol. Phys.* **9** 3023
Itikawa Y 1986 *Phys. Rep.* **143** 69
Jobe J D and St John R M 1967 *Phys. Rev.* **166** 117
Johnston A R and Burrow P D 1983 *J. Phys. B: At. Mol. Phys.* **16** 613
Joyez G, Huetz A, Pichou F and Mazeau J 1976 *Electron and Photon Interactions with Atoms* ed H Kleinpoppen and M R C McDowell (New York: Plenum) p 349
Mansky E J and Flannery M R 1990 *J. Phys. B: At. Mol. Opt. Phys.* **23** 4573
McConkey J W and Woosley J M 1969 *Proc. 6th Int. Conf. on Physics of Electronic and Atomic Collisions* (Cambridge, MA: MIT) Abstracts p 355
McEachran R P and Cohen M 1969 *J. Phys. B: At. Mol. Phys.* **2** 1271
Meneses G D and Csanak G 1987 *Z. Phys.* D **8** 219
Moussa M H R, de Heer F J and Schutten J 1969 *Physica* **40** 517
Nakazaki S, Berrington K A, Sakimoto K and Itikawa Y 1991 *J. Phys. B: At. Mol. Opt. Phys.* **24** L27
Opal C B and Beatty E C 1972 *J. Phys. B: At. Mol. Phys.* **5** 627
Phillips J M and Wong S F 1981 *Phys. Rev.* A **23** 3324
Pichou F, Huetz A, Joyez G, Landau M and Mazeau J 1976 *J. Phys. B: At. Mol. Phys.* **9** 933
Pochiat A, Roznel D and Peresse J 1973 *J. Physique* **34** 701

Rice J K, Truhlar D G, Cartwright D C and Trajmar S 1972 *Phys. Rev.* A **5** 762
St John R M, Miller F L and Lin C C 1964 *Phys. Rev.* A **134** 888
Sakai Y, Hirose N, Mori T, Min B S, Takayanagi T, Wakiya K and Suzuki H 1989 *Proc. 16th Int. Conf. on Physics of Electronic and Atomic Collisions (New York)* (Amsterdam: North-Holland) Abstracts p 192
Sakai Y, Suzuki T Y, Min B S, Takayanagi T, Wakiya K, Suzuki H, Ohtaui S and Takuma H 1991 *Proc. 17th Int. Conf. on Physics of Electronic and Atomic Collisions (Brisbane)* (Bristol: Hilger) Abstracts p 139
Showalter J G and Kay R B 1975 *Phys. Rev.* A **11** 1899
Skerbele A, Harshbarger W R and Lassettre E N 1973 *J. Chem. Phys.* **58** 4285
Spence D, Stuit D, Dillon M A and Wang R G 1983 *Proc. 8th Int. Conf. on Physics of Electronic and Atomic Collisions (Berlin)* Abstracts p 117
Suzuki H and Takayanagi T 1973 *Proc. 8th Int. Conf. on Physics of Electronic and Atomic Collisions (Belgrade)* Abstracts p 286
Thomas L D, Yarlagadda B S, Csanak G and Taylor H S 1973 *Comput. Phys. Commun.* **6** 316
Thomas L D, Csanak G, Taylor H S and Yarlagadda B S 1974 *J. Phys. B: At. Mol. Phys.* 7 1719
Trajmar S 1973 *Phys. Rev.* A **8** 191
Trajmar S and Register D F 1984 *Electron Molecule Collisions* ed K Takayanagi and I Shimamura (New York: Plenum) ch V
van Raan A E J, Moll P G and van Eck J 1974 *J. Phys. B: At. Mol. Phys.* 7 950
van Raan A E J, de Jough J P, van Eck J and Heideman H G M 1971 *Physica* **53** 45
van Zyl B, Dunn G H, Chamberlain G and Heddle D W O 1980 *Phys. Rev.* A **22** 1916
Vriens L, Simpson J A and Mielczarek S R 1968 *Phys. Rev.* **165** 7
Walters H R J 1984 *Phys. Rep.* **116** 1
Yagishita A, Takayanagi T and Suzuki H 1976 *J. Phys. B: At. Mol. Phys.* **9** L53